

Third International Symposium on the Effects of Surface Geology on Seismic Motion  
Grenoble, France, 30 August - 1 September 2006  
Paper Number: xxx

## FRONTIERS IN SOURCE MODELING FOR NEAR-SOURCE GROUND- MOTION PREDICTION

P. Martin Mai<sup>1</sup>, J. Ripperger<sup>1</sup>, J.-P. Ampuero<sup>1</sup>, and G. Hillers<sup>2</sup>

*1 Institute of Geophysics, ETH Zurich, 8093 Zurich, Switzerland*

*2 Institute for Crustal Studies, University of California, Santa Barbara, CA 93106-9630*

**ABSTRACT** Accurate prediction of the intensity and variability of strong ground motions for future large earthquakes depends on our ability to simulate realistic earthquake source models. While there has been considerable progress in characterizing the complexity of earthquake ruptures, recent devastating earthquakes have exhibited rather unexpected behavior. Moderate-size events occurred with surprisingly large ground motions, in contrast to very large ruptures that showed relatively low ground motions in the frequency range of 0.1 – 3.0 sec. These observations are at odds with standard ground-motion attenuation relationships, and fundamentally challenge current strong-motion prediction methods. A related issue is the question about the upper limits of near-source ground motions. These topics can only be reconciled by considering the complexity of earthquake faulting and the dynamic processes of rupture nucleation, propagation and arrest.

In this paper we discuss recent improvements to generate physically consistent earthquake rupture models for strong-motion simulation. We combine simulated slip distributions (realization of spatial random fields, consistent in scaling and spatial variability with slip distributions of past earthquakes) with constraints on the rupture nucleation and energy budget of earthquake rupture. Efficient stress-drop calculations in the spectral domain serve as input to estimate the temporal evolution of the rupture process through a set of empirical relationships derived from the analysis of spontaneous dynamic rupture models. Long-term earthquake-cycle simulations with realistic variability in rate-and-state friction parameters provide constraints on the generation, long-term behavior and characterization of earthquake source complexity for fault zones at different evolutionary stages.

The *pseudo-dynamic* source characterization is inherently kinematic, but emulates the most important characteristics of dynamic rupture. While the relationships between dynamic source parameters are simplifications of the true complexity in rupture physics, they help identify the interaction between source properties that are relevant for strong ground motion prediction, and provide an improvement over purely kinematic models.

### 1. Introduction

Accurate strong-ground motion prediction for future large earthquakes hinges on several key factors. Wave propagation from the earthquake source to the site of interest depends on the complexity of Earth structure, both deterministically as expressed in three-dimensional basin effects, and stochastically as modeled in scattering theory. Site effects in the shallow, near-surface structure underneath the observation site may lead to either

increased or decreased motions (compared to bed-rock level), and therefore further complicate strong-motion prediction. Complexity in the earthquake source adds another level of intricacy to ground-motion prediction methods. All these factors need to be incorporated into advanced strong-motion simulation approaches in order to be able to accurately predict not only the intensity, but also the variability of near-source ground motions.

While there has been considerable progress in strong-motion simulation methods for the frequency range up to about 1 Hz, one of the major challenges seismologists are facing is to calculate reliable near-source seismograms for frequency ranges of engineering interest ( $f > 10$  Hz). Earth structure, seismic source characterization, and site effects remain the key factors affecting high-frequency motions, but it is very difficult, if not impossible, to perform ground-motion simulations purely deterministically for high frequencies. Instead, at least some part of the simulation procedure needs to involve a stochastic component since Earth structure, and to some extent the earthquake source, is essentially unknown at the short spatial length scales needed for accurate high-frequency simulations. To account for the apparent stochastic nature of near-source acceleration time series, ground-motion simulation approaches used by earthquake engineers are for instance based on random-vibration theory (RVT), [Boore, 1983; Boore and Boatwright, 1984], but involve no physics in terms of the earthquake rupture and details on the wave-propagation. More advanced techniques combine deterministic low-frequency motions with a stochastic high-frequency signal [Irikura and Kamae, 1994; Pulido and Kubo, 2004; Pitarka et al., 1998, 2000], in which the stochastic part is meant to reflect the short-scale variability in source properties as well as the scattering of waves in the Earth. Recently, Hartzell et al. [2005] have combined realistic small-scale heterogeneity in the source properties with scattering operators for calculating broadband time histories, but found that the effects of scattering are somewhat masked by the heterogeneity in the kinematic source characterization.

There is also the question of what are the maximum credible ground-motions. This issue has become particularly critical when assessing the seismic hazard for structures and facilities planned for very long life spans which therefore require very long return periods. Standard empirical ground-motion attenuation relationships predict extremely large near-source motions for such return periods, and the question of the underlying physics and whether such motions ( $PGA > 5-10$  g;  $PGV > 5$  m/s) are possible are still unresolved. Realistic broadband simulation of near-source ground motion therefore remains the most challenging frontier in strong-motion prediction. Seismologists and earthquake engineers alike have to consider realistic heterogeneity in the source process, the dynamics of earthquake rupture, and in the complex propagation of the high-frequency wavefield in order to enhance our current capabilities in strong-motion calculations.

In the present paper we are mainly concerned with characterizing the complexity of earthquake sources. Over the past years we developed the *pseudo-dynamic* source model [Mai et al., 2001; Guatteri et al., 2003, 2004] based on a suite of dynamic rupture models whose target slip distributions are consistent with slip complexity found in past earthquakes [Mai and Beroza, 2002]. The temporal evolution of the rupture is constrained using empirical relationships derived from a large number of spontaneous dynamic rupture models, where we compute the static stress-drop based on a wave-number technique [Ripperger and Mai, 2004]. The point of rupture nucleation also exerts a large influence on the dynamics of earthquake rupture and hence ground-motion generation. We constrain the hypocenter position based on an analysis of hypocenter location in finite-source rupture models [Mai et al., 2005], in agreement with energy-budget considerations of dynamic rupture [Guatteri and Mai, 2003]. In order to understand how complexity on the rupturing fault is generated, we also perform earthquake-cycle simulations using a rate-

and-state friction formulation on a two-dimensional fault for which the rate-state-parameters are non-uniform. In particular, we investigate correlated along-strike heterogeneities in the critical length parameter  $L$  to mimic the behavior of smooth and rough (mature and young) faults [Hillers et al., 2006]. Moreover, through spontaneous dynamic rupture calculations for heterogeneous stress conditions we study the conditions for small earthquakes to grow into large events, the associated energy balance of the ruptures, and the source properties of the larger events (rupture speed, peak-slip velocities, stopping conditions).

## 2. Stochastic characterization of slip complexity in past earthquakes

Mai and Beroza [2002] used a spatial random field model to characterize the complexity of earthquake slip, described either in space by its autocorrelation function,  $C(r)$ , or in the spectral domain by its power spectral density,  $P(k)$ , where  $k$  is the wavenumber. Analyzing a set of 44 finite-source rupture models, Mai and Beroza [2002] found that a *von Karman* auto-correlation function, with correlation lengths  $a_x$ ,  $a_z$  that increase with magnitude, best represents the observed power spectral decay of earthquake slip models. The power spectral density  $P(k)$  of the *von Karman* auto-correlation function is given by

$$P(k) = \frac{4\pi H}{K_H(0)} \frac{a_x a_z}{(1+k^2)^{H+1}} \quad (1)$$

with  $k = \sqrt{a_x^2 k_x^2 + a_z^2 k_z^2}$ ;  $H$  denotes the Hurst exponent, and  $K_H$  the modified Bessel function of the first kind (order  $H$ ). The Hurst number  $H$  is found to be independent of magnitude,  $H = [0.8 - 1.0]$ . The scaling of the correlation lengths, displayed in Figure 1, is given by the following expressions:

$$a_x \approx 2.0 + 0.33 L_{\text{eff}} \quad \log(a_x) \approx -2.5 + 0.50 M_w \quad (2a)$$

$$a_z \approx 1.0 + 0.33 W_{\text{eff}} \quad \log(a_z) \approx -1.5 + 0.33 M_w \quad (2b)$$

where  $L_{\text{eff}}$ ,  $W_{\text{eff}}$  denote the effective source dimensions [Mai and Beroza, 2000]. In order to generate heterogeneous slip distributions for scenario earthquakes, we first constrain the fault dimensions based on source-scaling relations [e.g. Wells and Coppersmith, 1994; Somerville et al., 1999; Mai and Beroza, 2000]. Using Equation 2, we calculate the corresponding correlation lengths for which then the power-spectral density  $P(k)$  is computed. The two-dimensional slip function is finally obtained by adding random phase before carrying out the two-dimensional Fourier transform (under the requirement of Hermitian symmetry to ensure a purely real valued slip-function). The final slip function in space can then be tapered at the edges of the fault to avoid large slip values at the edges of the fault which are presumably unphysical since they lead to infinite large stress changes.

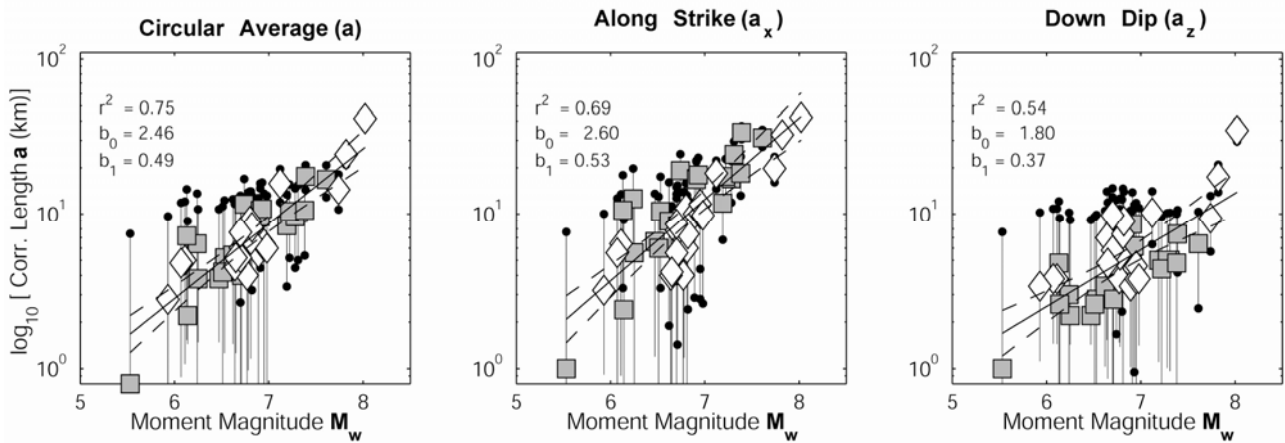


Figure 1: Scaling of correlation lengths with moment magnitude for the von Karman auto-correlation function. Correlation length  $a$  can be thought of an average of the along-strike and down-dip correlation lengths,  $a_x$  and  $a_z$ , respectively.

### 3. Pseudo-Dynamic Source Modeling Approach

#### 3.1. Fracture-energy scaling and rupture propagation

The pseudo-dynamic source model allows for constraining the temporal evolution of rupture consistent with rupture dynamics, in contrast to previous approaches in which local variations in rupture velocity or rise time were based on stochastic modeling [Hisada, 2000, 2001]. Our pseudo-dynamic approach is built on several relationships between rupture velocity, crack length, fracture energy and stress drop. For an anti-plane crack Andrews [1976] in a homogenous half-space derived an expression relation rupture resistance to shear-wave speed and rupture propagation velocity

$$1 - v^2 / \beta^2 = \pi^2 (R_c / 2)^2 \quad (3)$$

where the dimensionless parameter  $R_c$ , the rupture resistance, is given by

$$R_c = \mu G_c (\Delta\sigma^2 / L_h). \quad (4)$$

$G_c$  denotes fracture energy,  $v$  is rupture velocity,  $\beta$  is the shear-wave velocity,  $\mu$  is rigidity,  $\Delta\sigma$  is stress drop, and  $L_h$  denotes the crack length (distance from the hypocenter). Guatteri et al. [2003] showed that Equation 4 also approximately holds for 3D-dynamic rupture with realistic stress heterogeneity.

Based on spontaneous dynamic rupture modeling, Guatteri et al. [2004] developed an empirical linear relationship between fracture energy, crack length and stress drop, representing the growth of the stress-intensity factor with distance from the hypocenter (Figure 2a):

$$G_c = b_0 + b_1 \Delta\sigma L_h^{1/2} \quad (5)$$

where  $b_0$ ,  $b_1$  are magnitude- and faulting-style dependent regression coefficients. This approach has then be extended to a magnitude range  $6.4 \leq M_w \leq 7.2$ , based on a large number of dynamic models for strike-slip earthquakes (Guatteri et al., 2004), showing that

the regression coefficients need to be magnitude dependent:  $b_0 = 0.18$ ,  $b_1 = 0.0015$  if  $M_w \leq 6.5$ , while  $b_0 = 2.70$ ,  $b_1 = 0.0021$  if  $6.5 < M_w \leq 7.2$ . This relationship already suggests that larger earthquake require a faster fracture-energy increase in order to be energetically balanced and not to propagate and super-shear rupture velocities.

### 3.2. Fracture-energy scaling for surface-rupturing and buried earthquakes

In a recent study on the difference between observed and expected ground-motions for moderate-size to large earthquakes, Kagawa et al. (2004) reported the unexpected finding that large surface-breaking earthquakes had lower ground-motions (measured in terms of spectral acceleration) in a period range of engineering interest ( $0.2 < T < 3$  sec) than empirical attenuation relationships predicted. Conversely, moderate-size earthquakes that did not reach the surface (buried events) had larger ground-motions than empirically predicted. This controversial observation triggered a considerable debate about the causes for the lower motions for large surface-faulting ruptures, which eventually lead to the recent study by Mai et al. (2006) that investigated the scaling of fracture energy for a set of 12 dynamic rupture models for 9 different, well-recorded earthquakes.

Mai et al. (2006) used kinematic source inversions of these events, whose ground-motions were partly included in the database used by Kagawa et al. (2004), to develop fully spontaneous dynamic rupture models for these events that would match the kinematic inversion results and reproduce the observed strong-motions. In the subsequent statistical analysis, Mai et al. (2006) divided the set of rupture models into those events that did rupture the surface, and those that remained entirely buried earthquakes. Using the proposed fracture-energy scaling by Guatteri et al. (2004) (Eq. 5), they find that  $G_c$  scales markedly different between these two classes of earthquakes: fracture energy increases much more rapidly with the stress-intensity factor (stress drop  $\times$  sqrt (crack-length)) for surface rupturing events than for buried ruptures (Figure 2). The regression coefficients for the classes of events (referring to Eq. 5) are then given as  $b_0 = 0.2194$ ,  $b_1 = 0.0027$  for surface-rupturing events, and  $b_0 = 0.0802$ ,  $b_1 = 0.0016$  for sub-surface (buried) events.

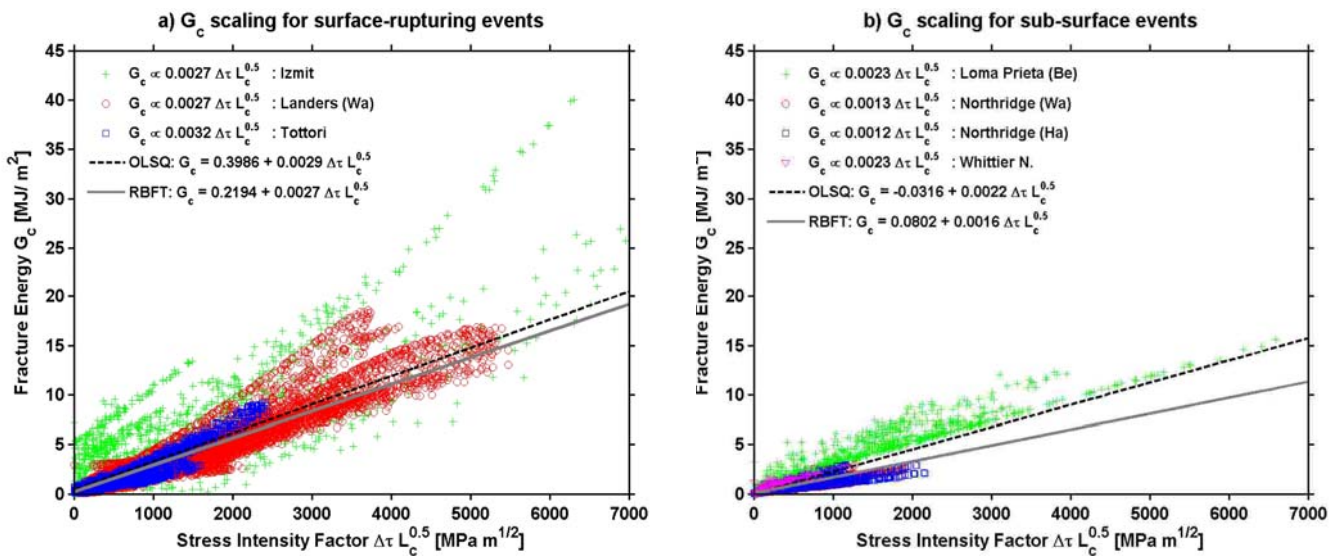


Figure 2: Fracture-energy scaling for surface-rupturing earthquakes (a, left) and buried ruptures (b, right), obtained from fully spontaneous dynamic rupture models of past earthquakes for which reliable kinematic source inversions and good strong-motion data exist.

Obviously, large surface-breaking earthquakes consume more fracture energy than moderate-size buried events during the expansion of the propagating crack front. It is important to note that fracture energy in this context contains not only the specific surface energy needed to create new crack surface in the framework of linear elastic fracture mechanics, but also comprises contributions from other dissipative processes at the crack tip, like heat, micro-cracking, off-fault yielding etc. The “seismological” fracture energy  $G_c$  is therefore an integral meso-scopic energy measure that combines micro-scopic and meso-scopic dissipation processes in the volume around the expanding crack front, which is also reflected in the standard slip-weakening model (Andrews, 1976) used in many dynamic modeling studies. Formulating a simplified energy-balance equation for earthquake rupture – existing strain energy is converted to fracture energy and seismic radiation – therefore suggests that large fracture-energy consumption would lead to lower seismic radiation. Although this energy consideration is somewhat approximate, it captures the most important aspects of dynamic rupture and ground-motion excitation. The observation that large-surface rupturing earthquakes caused lower-than-expected near-field motions can therefore be reconciled by the higher fracture-energy consumptions of these events. Since empirical ground-motion attenuation relationships are developed based on mostly moderate-size events, these large earthquakes have been under-represented in the respective databases, leading to the lower expectation. Current updates and revisions of empirical ground-motion relations in fact include the efforts to account for rather low near-source motions for large surface-breaking earthquakes.

### 3.3. Rise-time distributions and dynamically consistent source-time function

The pseudo-dynamic method also comprises an approximation to the on-fault slip-velocity function, modeled as two over-lapping triangles (Figure 4a) that are given by an isosceles triangle of height  $V_{max}$  (peak-slip velocity) and base  $T_p$  (pulse width), while the second rectangular triangle is of height  $V_{max}/2$ . The total length of this slip-velocity function is given by the rise time,  $\tau_r$ . The analysis of our dynamic rupture models suggests that  $V_{max}$  can be calculated from a similar expression as given in Day [1982]:

$$V_{max} = 0.5 V_{maxref} W T_p v / \beta \mu. \quad (6)$$

where  $W$  denotes the fault width and  $V_{maxref}$  represents a reference peak-slip velocity. In order to generate a dynamically consistent rupture model, i.e. a physically realizable spatio-temporal rupture evolution for a simulated slip distribution, we first deploy Equation 5 to compute fracture energy (using the appropriate regression coefficients), which we then insert into Equation 3 and 4 to calculate the rupture propagation, and hence rupture onset-times, over the fault plane. The pulse-width  $T_p$  and the slip-rise time,  $\tau_r$ , are then computed in a two-step process such that their distributions are consistent with the results found in our spontaneous dynamic rupture models. Figure 5 displays the application of the pseudo-dynamic approach to the simulation of scenario ruptures of magnitude 7.2 strike-slip earthquakes [Miyake et al, 2004].

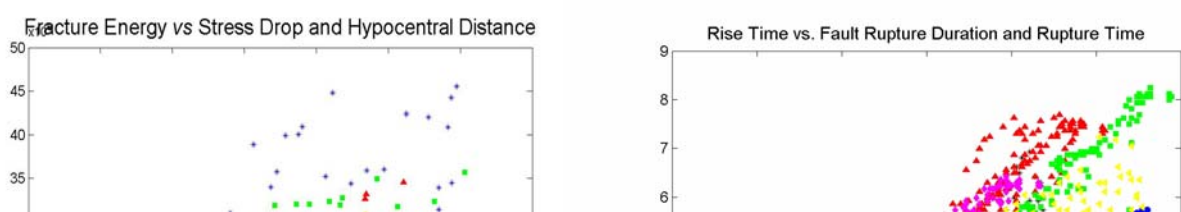


Figure 3 (a, left) Fracture energy values as a function of stress drop and crack distance for 6 simulated strike-slip earthquakes ( $M=7.0$ ), according to Guatteri et al. [2003]. (b, right) Scaling of dynamically inferred rise times ( $\tau_r$ ) with respect to the total rupture duration for the same set of 6 strike-slip events.

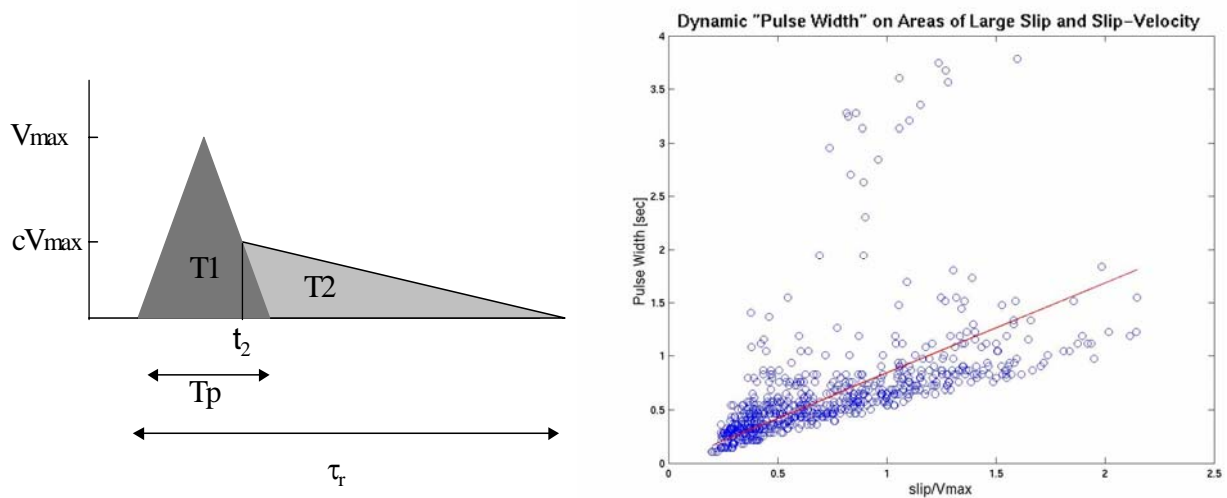


Figure 4: Slip-velocity function parameterization in the pseudo-dynamic approach, characterized by two overlapping triangles, an isosceles triangle T1 and a rectangular triangle T2 (left), and the scaling of pulse width  $T_p$  (right). The scaling of the parameter rise time  $\tau_r$  is shown in Figure 3.

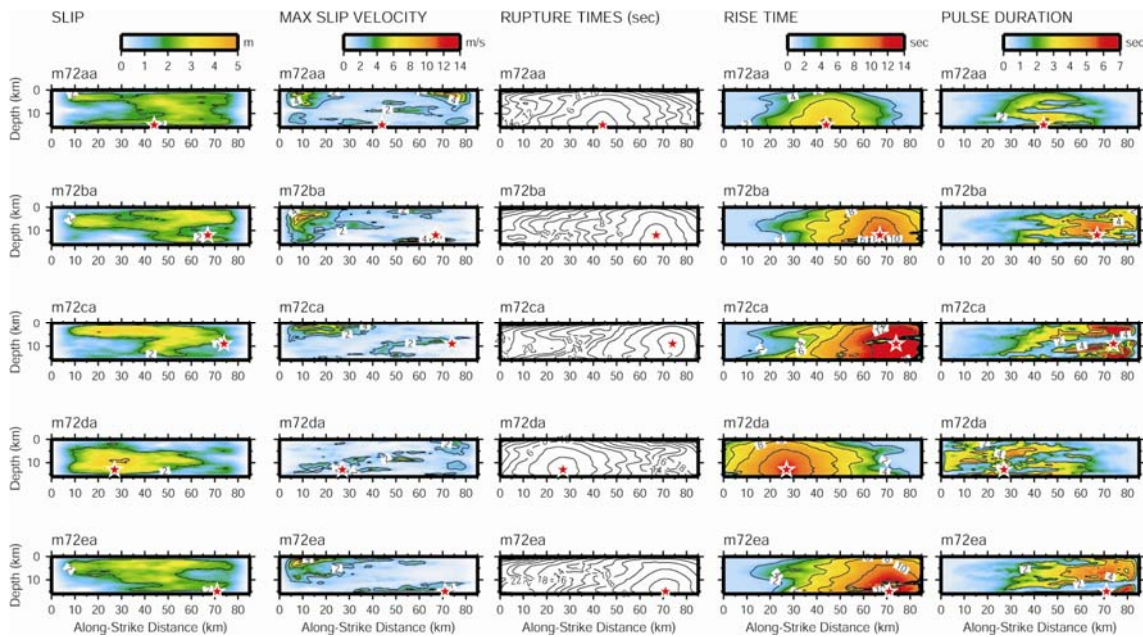


Figure 5: Pseudo-dynamic source models for magnitude 7.2 strike-slip scenario earthquakes [Miyake et al. 2004]. The rupture models display a large degree of spatial variability in all source parameters, consistent with source inversions of past earthquakes as well as dynamic rupture modeling results.

#### 4. Constraints on hypocenter location in the presence of slip/stress complexity

While the spatial complexity of earthquake slip has been studied both theoretically and by analyzing the inferred slip distributions of past earthquakes, the hypocentral position with respect to the final slip has received little attention. However, the position of the hypocenter, both with respect to the overall fault dimensions and the small-scale variability in slip (or stress) on the fault, greatly affects ground motion generation as well as the propagation conditions for dynamic rupture. Using a database of more than 80 finite-source rupture models [Mai, 2004] for more than 50 earthquakes ( $M_w = 4.1-8.1$ ) with different faulting styles occurring in both crustal and subduction environments, Mai et al. [2005] analyzed the location of the hypocenter within the fault and considered the correlation between hypocenter location and regions of large slip.

One of their key conclusions states that rupture can nucleate at locations with any level of relative displacement, indicated by the statistical distributions of the ratios of the hypocentral slip to either the average or the maximum slip. They also find that rupture nucleates in regions of very large slip ( $D \geq 2/3 D_{max}$ ) in only 16% of the events, in regions of large slip ( $1/3 D_{max} < D < 2/3 D_{max}$ ) in 35% of the events, and in regions of low slip ( $D \leq 1/3 D_{max}$ ) in 48% of the events. For the latter population, however, the hypocenters are located in close proximity to a region of large slip. Taken together, Mai et al. [2005] suggest that ruptures may nucleate in regions of low slip, but tend to nucleate close to regions of large slip. Earthquake ruptures then need to encounter a zone of very large slip within half the total rupture length (Figure 6) in order to grow into a large earthquake. These conditions on the hypocenter locations are consistent with simplified energy-budget considerations for dynamic rupture models, and can in fact be verified by means of spontaneous dynamic rupture calculations.

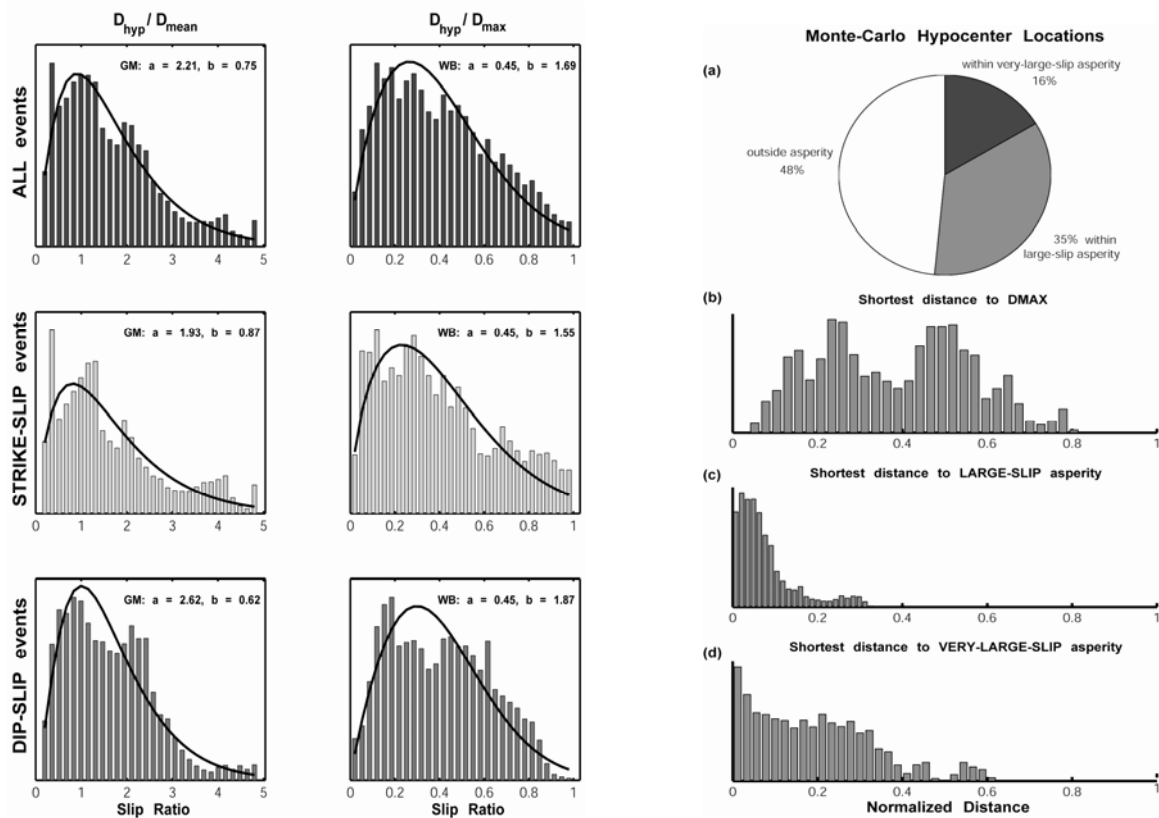


Figure 6: Left: Distributions of slip at the hypocenter ( $D_{hyp}$ ), normalized by the mean displacement ( $D_{mean}$ ) and maximum slip displacement ( $D_{max}$ ); thick black lines indicate best-fitting distribution functions with respective coefficients  $A$ ,  $B$  (GM: Gamma distribution; WB: Weibull distribution). Right: Monte-Carlo-simulated distribution of the various distance measures, normalized to the maximum rupture distance, showing that earthquakes need to encounter a large-slip asperity in very close distance, and a very-large-slip (high stress drop) region with half of the maximum rupture distance.

## 5. Dynamic simulations with constrained stochastic initial stress

In this line of research, we investigate how the evolution of dynamic earthquake rupture is controlled by heterogeneous stress distributions on the fault plane. We generate initial, heterogeneous stress condition, then ruptures are initiated at randomly chosen hypocenters and their evolution is tracked in space and time, allowing us to study in detail the conditions required for rupture to grow from small into large events. The results aid in better understanding the relations between hypocenter location and large-slip (high-stress-drop) regions, and provide important insight into the conditions on the fault that govern the rupture velocity and rise time, all of which have a large influence on the resulting near-source ground motions.

We use a 3D finite difference code to model rupture on a single vertical fault plane obeying a slip-weakening friction law. The friction parameters (critical slip-weakening distance, coefficients of friction) are kept homogeneous over the fault plane, whereas the distributions of shear and normal stress are modeled as spatial random fields with predefined wavenumber spectra. We test different parameterizations for the stress distributions, being either purely fractal (with variable fractal dimension  $D$ ) or following a

von-Karman auto-correlation function (with variable correlation lengths). We also investigate how the degree of correlation between shear and normal stress affects the spontaneous dynamic rupture calculations.

Figure 7 displays a realization of a random initial stress field. Here we chose a fractal dimension  $D = 1$  with a corner wavenumber  $k_c = 0.2 \text{ km}^{-1}$ ; the resulting stress field is then scaled to be in the range of 10-30 MPa. Assuming a slip-weakening friction law, we model the yield stress as being correlated with shear stress, such that high relative strength is assumed in low stress drop regions (similar to Oglesby and Day, 2000). We assume a constant coefficient of friction, and then adjust the initial shear stress such that it cannot be lower than sliding friction. The fault boundaries are unbreakable, and constrained to be  $15 \times 20 \text{ km}$ . The dynamic calculations are carried out for constant slip-weakening distance  $D_c = 0.1 \text{ m}$ , a grid spacing of 100 m, and a homogeneous half space. We place 48 hypocenters on the fault plane, and terminate the calculations once the slip-velocity falls below a certain threshold. Only 3 out of 48 rupture nucleation points resulted in rupture growth beyond the initial zone of forced failure, indicating that the conditions for generating large earthquakes depends very subtly on the spatial relations between hypocenter and stress conditions on the fault.

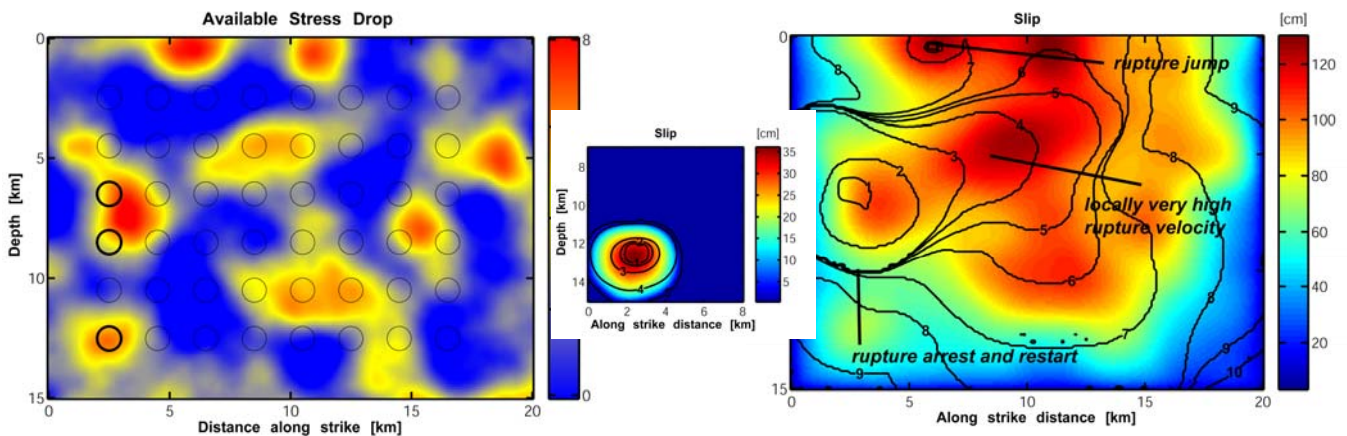


Figure 7a: Initial stress distribution with 48 potential hypocenters (circles) used in spontaneous dynamic rupture calculations. Only the thick-black circles resulted in rupture that grew outside their nucleation patch. The small event (center) shows the rupture that started in the lower-most left corner, the large-scale event (right) nucleated at the top-most black-circle, rupturing the entire fault plane.

Figure 7b, c then show two of the 3 “successful” earthquakes resulting from the stress field shown in Figure 7a. While the small earthquake ( $M_w = 5.3$ ) remains essentially a circular patch, stopped by the surrounding low-stress-drop regions, the large rupture ( $M_w = 6.6$ ) displays a large degree of rupture complexity, although the initial conditions at rupture nucleation do not appear to be very different from those for the small earthquake. In Figure 7c, we observe regions where rupture almost stopped, and then started again, zones of very high rupture velocity, and even a region of rupture jumping. This very complicated rupture behavior will strongly affect the near-source ground motions generated by such an earthquake, and our future work will target this effects. Our current results strongly reinforce the finding from Section 5, namely, that the rupture nucleation point is in fact a very delicate point for which the instability conditions for further rupture growth depend very strongly on the stress conditions in the immediate vicinity.

To further investigate rupture nucleation and propagation in heterogeneous stress regimes, we devised a procedure to mimic tectonic loading acting on simulated stress

distributions and let rupture physics define where the most likely nucleation point would be (Ripperger et al., 2006). We find that the nucleation patch size can be approximated according to the work by Uenishi and Rice (2003); moreover, the rupture trajectory and its ability to grow (a) outside the nucleation patch, (b) to grow into a moderate-size events, or (c) to become a system-wide large earthquake depends crucially on the underlying stress distribution (i.e. its fractal dimension, standard deviation and cut-off wave-number). Figure 8 shows example stress distributions (for variable heterogeneity), while Figure 9a summarizes the rupture-size distributions we obtain for a given heterogeneity class and variable S-parameter (defined as the ratio of strength excess and stress drop).

Interestingly, our large set of simulations with heterogeneous stress distributions returns on overall moment-area scaling that is close to the classical constant average stress-drop scaling as proposed by Kanamori & Anderson (1975) (Figure 9b). The diversity of earthquake dynamics, when looked upon at a macroscopic scale, can be explained by a very simple (constant stress-drop) scaling model, glossing over many important details of the rupture process which will strongly affect the near-source ground motions. Conversely, the use of scaling relations based on macroscopic source parameters for ground-motion prediction will be overly simplistic since rupture dynamics calls for a very large variability in the source process and hence the resulting ground motions. It is therefore strongly advisable to incorporate as much rupture physics as possible into the source characterization for ground-motion simulation studies.

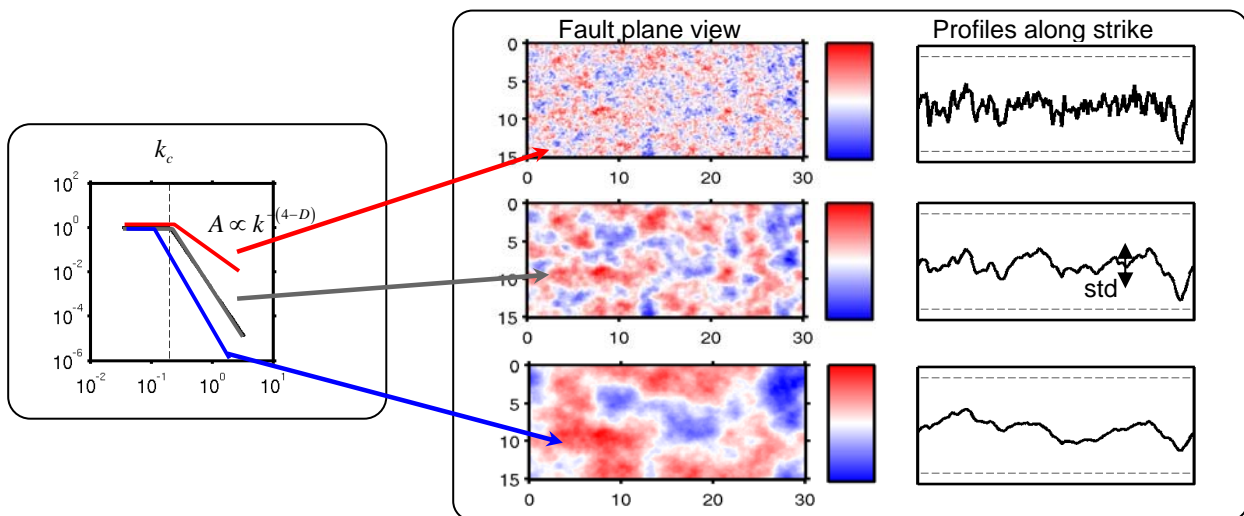


Figure 8: Examples for heterogeneous stress drop distributions, generated with the same random phase, but different wave-number decay. The spectral decay is characterized by the fractal dimension,  $D$ , and the corner wavenumber,  $k_c$ . The last model parameter for the stress distributions is given by the standard deviation.

## 6. Earthquake-cycle simulations with heterogeneity in rate-and-state friction

Another important line of modeling for better understanding earthquake processes and the associated strong-motion generation addresses the question of how rupture complexity is generated in the first place, and whether it persists over multiple earthquake cycles. To that end, we perform earthquake-cycle simulations with variability in the rate-and-state parameters, including along-strike correlations lengths that mimic different evolutionary stages of faults, from young, complex, and hence “rough” faults (with a large

degree of small-scale variability in rate-and-state parameter  $L$ ) to mature faults that are “smooth” (for which  $L$  correlates over long distances).

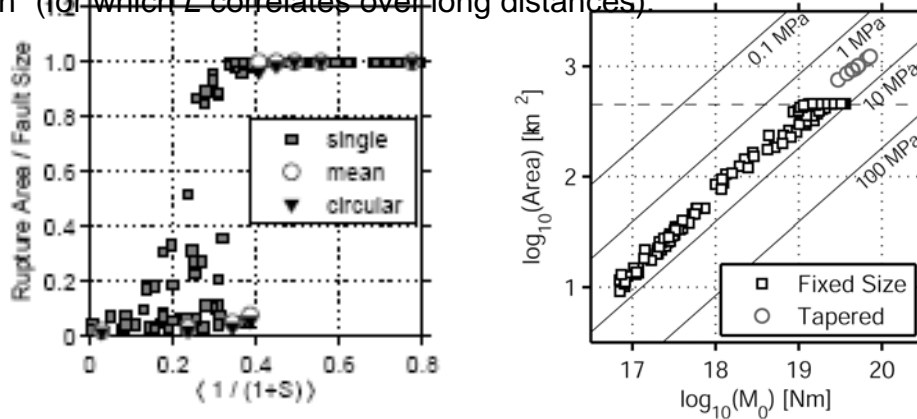


Figure 9: Left: Ruptured area for all simulations with  $D = 2$  and  $kc = 0.2 \text{ km}^{-1}$  and varying standard deviation ( $std$ ) plotted versus average stress level. Rupture area is normalized by fault size. The white circles represent runs where the initial stress is the mean of 10000 individual realizations, aligned at their stress maximum. For these mean stress functions the sharp transition from small to system-wide ruptures is clearly visible. Black triangles indicate predictions for the mean stress fields of a simplified model assuming circular mode I cracks. Right: Moment-area scaling for  $N = 420$  dynamic simulation with heterogeneous stress drop. Despite various degrees of heterogeneity, the overall scaling is surprisingly simple.

Previous studies of slip on a fault governed by rate-and-state friction [e.g., Rice, 1993; Ben-Zion and Rice, 1995, 1997; Tullis, 1996; Lapusta et al., 2000] employed frictional properties that correspond to a fairly homogeneous smooth fault. In most cases, the only types of heterogeneities were the lab-based variations of the parameters  $a$  and  $b$  that produce transitions between velocity strengthening and velocity-weakening regimes. In addition to depth-variations of  $a$  and  $b$ , we use correlated heterogeneities of the critical slip distance parameter  $L$  to model a form of geometrical heterogeneities on a fault that is related to roughness. Our model setup follows the quasi-dynamic approach of Rice [1993] in the continuum limit, in which a rate/state controlled 2D fault plane is embedded in a homogeneous, elastic half space.

More specifically, we perform 3D quasi-static as well as quasi-dynamic simulations with a family of 2D anisotropic correlated distributions of  $L$  having different correlation lengths along strike and with depth. The depth-variation of  $L$  is chosen to reflect an overall reduction of the gouge thickness (and hence  $L$ ) with depth. The variations of  $L$  along strike provide an approximate representation of faults that are at different evolutionary stages. Relatively smooth mature faults like the San Andreas are represented with distributions that have large horizontal correlation length, while distributions with small correlation lengths are used to represent rougher immature faults like the San Jacinto and faults in the eastern CA shear zone. The choices of representative correlation lengths is guided and constrained by maps of fault structures of the type compiled by Wesnousky [1994], and by the compilation of inverted slip histories [Mai, 2004]. Our 3D code handles various cases of anisotropic correlated distributions of  $L$  that we study in order to analyze (1) Nucleation and arrest properties of failure episodes on a heterogeneous fault governed by RSD friction. (2) Comparison between properties of final simulated slip histories and those

of the inverted slip histories [Mai, 2004]. (3) Frequency-size and temporal statistics of simulated earthquakes on a heterogeneous fault governed by RSD friction.

For brevity, we will focus on two specific case studies here without going into the numerical details of the method which is presented in Hillers et al. [2006]. We first perform several calibration calculations to understand the generic response of the system to heterogeneities in the friction parameters. The first one uses a depth-dependent  $a-b$  profile (with two velocity-strengthening regions,  $a-b > 0$ , at the top and bottom of the modeled fault), and a critical slip distance  $L$  that is constant throughout the plane. The generic model response in this case is a regular stick-slip behavior. The second calibration calculation involves a constant  $a-b$  profile, but a depth-dependent distribution of  $L$ . Here we also find stable fault behavior (i.e. regular stick-slip) if  $L$ -values below the seismogenic zone are sufficiently large.

The interesting fault behavior occurs when the  $L$ -values follow a random uniform distributed over the fault plane (within a specified range, see Figure 10). Depending on the maximum value of  $L$  in each case, we find either a rather stable response of the fault (Figure 10, right; maximum  $L$  high), where smaller and larger events occur relatively fixed in time and space. If the maximum  $L$  value is chosen small, the fault's response is more complex (Figure 10, left). Larger and smaller events occur interspersed in space and time with considerable variability in size (magnitude), position and time of occurrence. Figure 11 shows a collection of final-slip maps for a range of magnitudes, along with the hypocenter positions. The slip maps clearly show similar slip complexity as imaged in finite-source rupture models [Mai, 2004], and the location of rupture nucleation (close to large slip areas) is consistent with the findings by Mai et al. [2005] and energy-budget considerations of dynamic rupture.

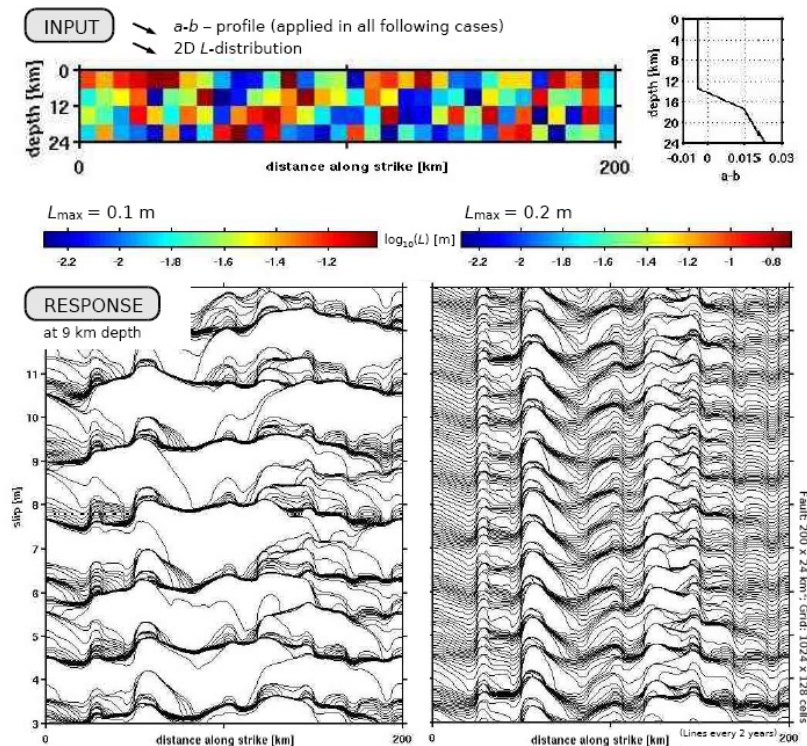
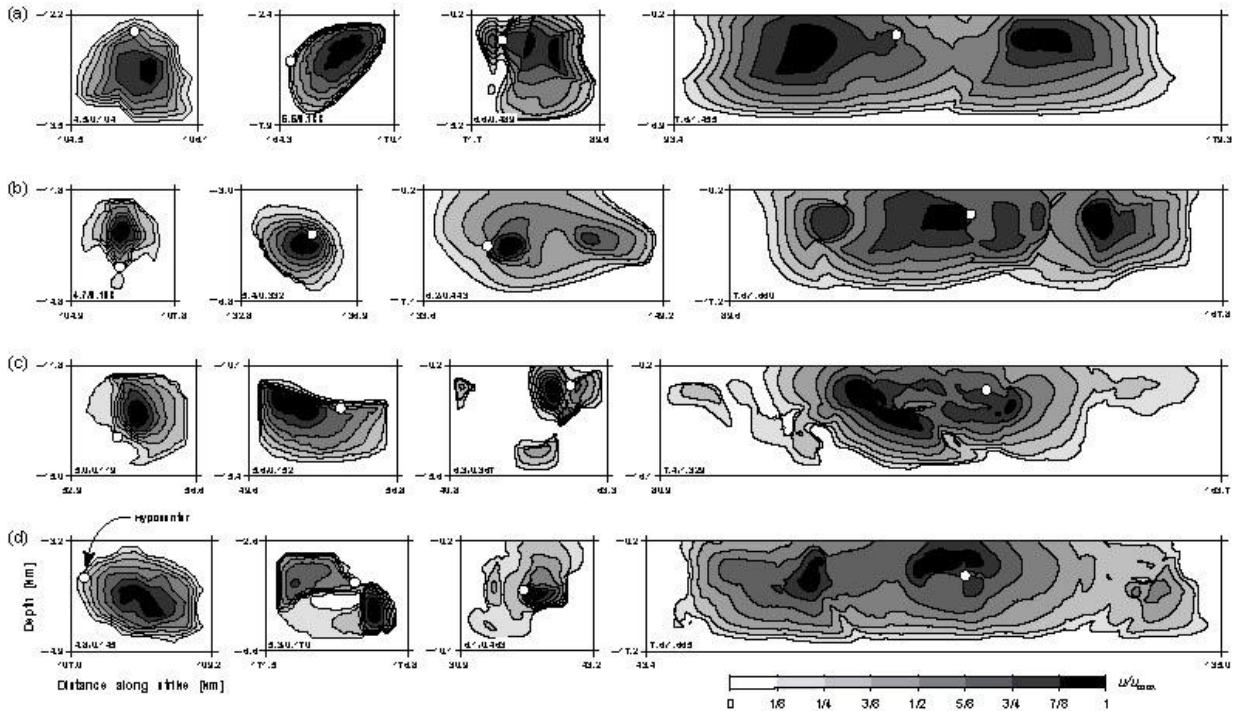


Figure 10: (top-left) Input chessboard pattern with spatially variable  $L$ -values on a two-dimensional strike-slip fault. (top-right) Input  $a-b$  profile for this set of calculations. (bottom-left) Response of the system for an  $L$ -distribution with  $L_{max} = 0.1$  m. (bottom-right) Response of the system for an  $L$ -distribution with  $L_{max} = 0.2$  m. In general we observe that a fault

with heterogeneous 2D  $L$ -distributions can produce a broad range of event sizes whose statistics approach Gutenberg-Richter-type relations. We find that larger applied



$L$ -values result in a more stable response of the fault response.

Figure 11: Maps of final slip on the fault plane from multi-cycle simulations for events of various source size and magnitude (increasing from left to right). The white dot in each diagram marks the rupture nucleation point, located near the edges of high-slip patches.

Finally, using a set of model-quakes generated by our multi-cycle simulations, we apply the *pseudo-dynamic source parameterization* to the final slip maps (similar to what is shown in Figure 11) in order to compute source models for ground-motion calculations. Figure 12 shows a selection of rupture models and the resulting maps of ground-motion intensity (here PGV and PGA for a maximum frequency  $f_{\max} = 1$  Hz) for two scenario events. In this application, the rupture models are resolved onto the Central Marmara Fault in the Marmara Sea (Turkey), just west of the mega-city Istanbul. This segment of the North Anatolian Fault (NAF) has not ruptured during the last  $\sim 250$  years, but has produced two sizable earthquakes ( $M \sim 7.2$ ) in 1766. Ground-motions are computed for a one-dimensional velocity-density model (R. Gok, written communication), assuming a vertical fault of 100 km length and 18 km down-dip width (whereby the actual length and width of the rupture could be smaller, according to whatever source-size the particular multi-cycle source-model realization would provide), using a discrete-wavenumber integration method (Spudich and Xu, 2002). The ground-motion intensity maps clearly show the distinct directivity pattern expected for large, unilateral ruptures, while the variability due to source effects adds significant local variations to the resulting ground shaking. For a large number of scenario simulations one can therefore expect very large ground-motion variability that ultimately should be reflected in (probabilistic) seismic hazard analysis.

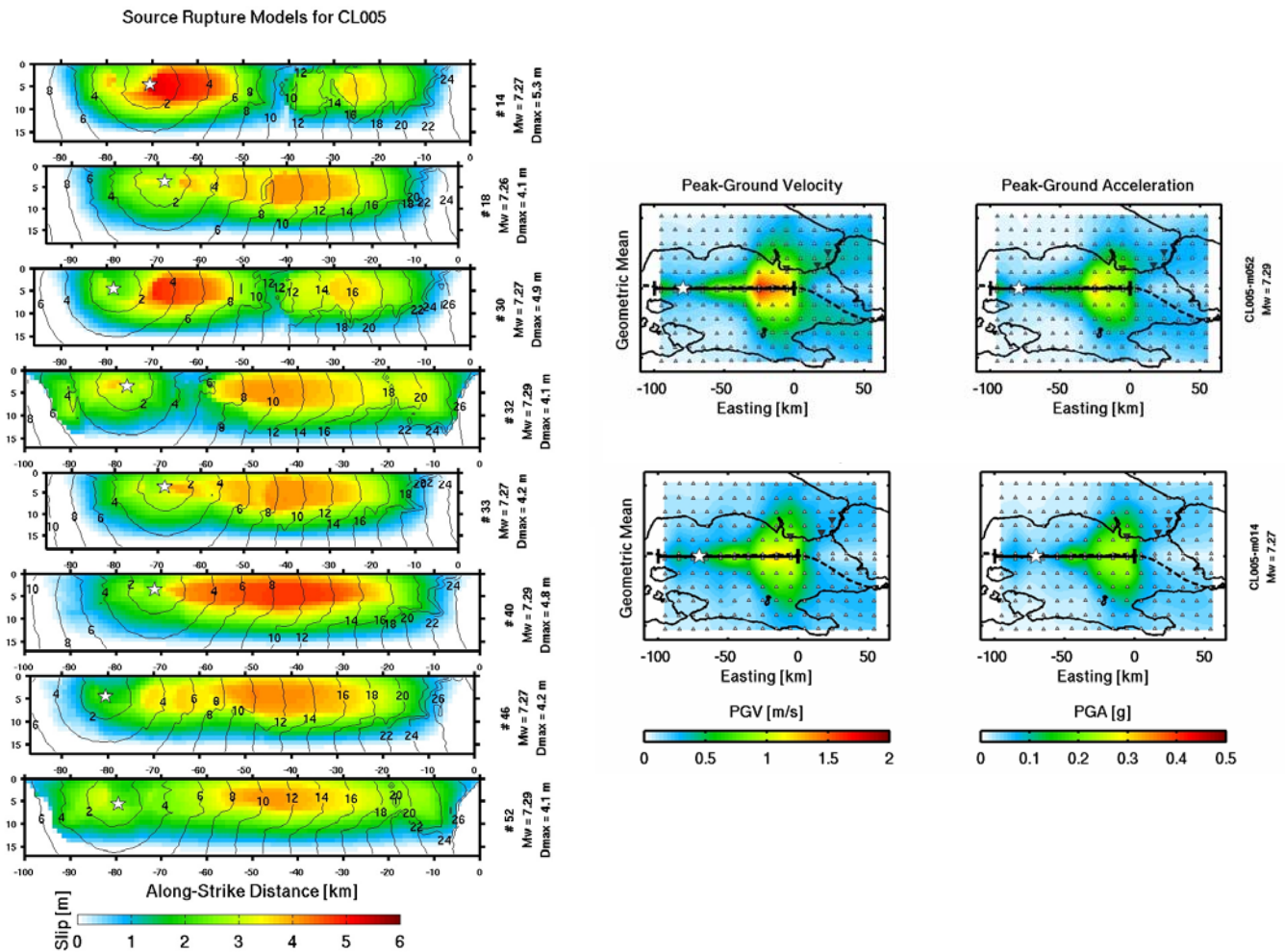


Figure 12: Left: Earthquake source models with slip distributions from multi-cycle simulations. The spatio-temporal evolution (rupture velocity and rise time) is then computed following the pseudo-dynamic approach (Section 3). Right: Ground-motion maps (PGV, left; PGA, right) for two of the rupture models, resolved on the Central Marmara Fault west of Istanbul (Turkey). The ground-motion intensities ( $f_{max} = 1$  Hz) clearly show the strong directivity effect, but also the variability in the source models.

## 7. Conclusions

In this paper we outlined our current approaches to push the frontiers of near-source strong motion prediction towards uncharted terrain, involving modeling of realistic slip complexity (Section 2), dynamically consistent spatio-temporal source characterization (Section 3). Section 4 illustrates the conditions on hypocenter locations, and these tools taken together already provide a large step forward for generating realistic source models for ground-motion calculations. In Section 5 and 6 we present our current approach to better understand the physical principles that govern, generate, and maintain rupture complexity, both for individual ruptures with heterogeneous initial conditions (Section 5) and for multiple scenario earthquakes generated through earthquake-cycle simulations with variability in the rate-and-state parameters (Section 6).

Our future work will further address the space-time complexity of events in earthquake-cycle calculations, controlled by the critical slip distance  $L$ , resulting in either rather predictable fault responses (if the maximum  $L$  is large) or very complex fault response (if the maximum  $L$  is small). We also continue to investigate the details of the rupture process of individual scenario earthquakes, both from earthquake-cycle simulations and generated in spontaneous dynamic rupture calculations for heterogeneous initial stress/strength conditions.

These (quasi-)dynamic scenario earthquakes represent complex sources for which near-source ground motions can be readily calculated using a variety of methods (1D or 3D, including layered or more complicated 3D velocity structures). We have shown the potential use of multi-cycle simulations for generating ground-motion maps (so far at low frequencies only, neglecting scattering and other high-frequency effects) that ultimately can be used for seismic hazard purposes. To that end, the computational pathway from simulating individual dynamic ruptures to multi-cycle simulations to ground-motion calculations, may offer the possibility to establish simulation-based probabilistic seismic hazard to supplement (and potentially improve) current practice of near-source seismic hazard assessment.

## 8. References

- Andrews, D.J. (1976). Rupture propagation with finite stress in antiplane strain, *J. Geophys. Res.*, 81, 3575-3582.
- Andrews, D. J. (1980). A stochastic fault model 1. Static case, *J. Geophys. Res.*, **85** (B7), 3867–3877.
- Ben-Zion, Y., and J.R. Rice (1995). Slip Patterns and Earthquake Populations Along Different Classes of Faults in Elastic Solids, *J. Geophys. Res.*, **100** (B7), 12959-12983.
- Ben-Zion, Y., and J.R. Rice (1997). Dynamic simulations of slip on a smooth fault in an elastic solid, *J. Geophys. Res.*, **102** (B8), 17771-17784.
- Beroza, G.C., and P. Spudich (1988). Linearized inversion for fault rupture behavior; application to the 1984 Morgan Hill, California, earthquake, *J. of Geophys Res.*, **93** (6), 6275-6296.
- Boore, D.M. (1983). Stochastic simulation of high frequency ground motions based on seismological models of the radiation spectra. *Bull. Seismol. Soc. Am.* **73**, 1865– 1894.
- Boore, D.M., Boatwright, J. (1984). Average body-wave radiation coefficients. *Bull. Seismol. Soc. Am.* **74** (5), 1615–1621.
- Bouchon, M. (1997). The state of stress on some faults of the San Andreas system as inferred from near-field strong motion data, *J. Geophys. Res.*, **102** (B6), 11,731–11,744.
- Day, S.M. (1982). Three-dimensional simulation of spontaneous rupture: The effect of nonuniform prestress, *Bull. Seismol. Soc. Am.*, **72**, 1,881-1,902.
- Guatteri, M., and P.M. Mai (2003). The energy budget of earthquake rupture: a view from spontaneous rupture modeling and finite-source models, *EOS Trans. AGU*, **84** (46), *Fall Meet. Suppl., Abstract S42C-0188*.
- Guatteri, M., P.M. Mai, G.C. Beroza, and J. Boatwright (2003). Strong ground-motion prediction from stochastic-dynamic source models, *Bull. Seismol. Soc. Am.*, **93** (1), 301-313.
- Guatteri, M., P.M. Mai, and G.C. Beroza (2004). A pseudo-dynamic approximation to dynamic rupture models for strong ground motion prediction, *in press Bull. Seismol. Soc. Am.*
- Hartzell, S., M. Guatteri, P.M. Mai, P-C. Liu and M. Fisk (2004). Calculation of Broadband Time Histories of Ground Motion: Part II, Kinematic and Dynamic Modeling with Theoretical Green's Functions, *submitted to Bull. Seis. Soc.*
- Hillers, G., Y. Ben-Zion, and **P.M. Mai**, (2006). Seismicity on a fault controlled by rate-and-state dependent friction with spatial variation of the critical slip distance, *J. Geophys. Res.*, doi:10.1029/2005JB003859.
- Hisada, Y. (2000). A theoretical omega-square model considering the spatial variation in slip and rupture velocity, *Bull. Seism. Soc. Am.* **90**, 387-400.
- Hisada, Y. (2001). A theoretical omega-square model considering the spatial variation in slip and rupture velocity Part 2: Case for a two-dimensional source model, *Bull. Seism. Soc. Am.* **91**, 651-666.

- Irikura, K., and K. Kamae (1994). Estimation of strong ground motion in broad-frequency band based on a seismic source scaling model and an empirical Green's function technique, *Annali Di Geofisica* **37**, 1721-1743.
- Kagawa, T., K. Irikura, and P. G. Somerville (2004). Differences in ground motion and fault rupture process between the surface and buried rupture earthquakes. *Earth Planets and Space* 56(1): 3-14.
- Kanamori, H., and D. L. Anderson (1975), Theoretical basis of some empirical relations in seismology, *Bull. Seis. Soc. Am*, **65**, 1073-1095.
- Lapusta, N., J.R. Rice, Y. Ben-Zion, and G.T. Zheng (2000). Elastodynamic analysis for slow tectonic loading with spontaneous rupture episodes on faults with rate- and state-dependent friction, *J. Geophys. Res.*, **105** (B10), 23765-23789.
- Mai, P. M., and G. C. Beroza (2000). Source scaling properties from finite-fault-rupture models, *Bull. Seism. Soc. Am.*, **90**, 604-615.
- Mai, P.M., and G.C. Beroza (2002). A spatial random field model to characterize complexity in earthquake slip, *J. Geophys. Res.*, **107** (B11), 2308, doi:10.1029/2001JB000588.
- Mai, P.M. (2004). Online database of finite-source rupture models, <http://www.seismo.ethz.ch/srcmod>.
- Mai, P.M., P. Spudich, and J. Boatwright (2005). Hypocenter locations in finite-source rupture models, *Bull. Seis. Soc. Am.*, Vol 95 (3), 965-980
- Mai, P.M., P. Somerville, A. Pitarka, L. Dalguer, H. Miyake, G. Beroza, S.-G. Song, K. Irikura (2006). Fracture-energy scaling in dynamic rupture models of past earthquakes, *in revision for AGU Chapman Monograph Series on Radiated Seismic Energy* (edited by A. McGarr, R. Abercrombie, H. Kanamori).
- Miyake, H., P.M. Mai, and G.C. Beroza (2004). Pseudo-Dynamic Rupture Characterization: Insights from Near-Source Ground Motion Simulations, and Recent Updates, SSJ-meeting in Fukuoka, poster S08-08162054-8441A.
- Oglesby, D.D., and S.M. Day (2002). Stochastic fault stress: Implications for fault dynamics and ground motion, *Bull. Seis. Soc. Am.*, **92** (8), 3006-3021.
- Okada, Y. (1992), Internal deformation due to shear and tensile faults in a half-space, *Bull. Seism. Soc. Am.*, **82** (2), 1018–1040.
- Pitarka, A., Irikura, K., Iwata, T., Sekiguchi, H. (1998). Three-dimensional simulation of the near-fault ground motion for the 1995 Hyogo-ken Nanbu (Kobe), Japan, Earthquake. *Bull. Seismol. Soc. Am.* **88** (2), 428– 440.
- Pitarka, A., Somerville, P., Fukushima, Y., Uetake, T., Irikura, K., (2000). Simulation of near-fault strong-ground motion using hybrid green's function. *Bull. Seismol. Soc. Am.* **90** (3), 566– 586.
- Pulido, N. and T. Kubo (2004). Near-fault strong motion complexity of the 2000 Tottori earthquake (Japan) from a broadband source asperity model, *Tectonophysics* **390**, 177– 192.
- Rice, J.R. (1993). Spatiotemporal Complexity of Slip on a Fault, *J. Geophys. Res.*, **98** (B6), 9885-9907.
- Ripperger, J. and P.M. Mai (2004). Fast computation of static stress changes on 2D faults from final slip distributions, *Geophys Res. Lett.* VOL. 31, L18610, doi:10.1029/2004GL020594.
- Ripperger, J., P.M. Mai, and J.-P. Ampuero (2006). Nucleation, propagation and arrest of dynamic rupture under constrained stochastic stress: implications for earthquake scaling and near-source ground motions, *submitted to J. Geophys. Res.*
- Spudich, P., and L. Xu (2002), Software for calculating earthquake ground motions from finite faults in vertically varying media., in *International Handbook of Earthquake and Engineering Seismology*, edited by W. H. K. Lee, Kanamori, H., Jennings, P., Kisslinger, C., Academic Press, Orlando.
- Tullis, T.E. (1996). Rock friction and its implications for earthquake prediction examined via models of Parkfield earthquakes, *Proceedings of the National Academy of Sciences of the United States of America*, **93** (9), 3803-3810.
- Wesnousky, S.G. (1994). The Gutenberg-Richter or Characteristic Earthquake Distribution, Which Is It, *Bull. Seis. Soc. Am*, **84** (6), 1940-1959.